Biochemistry and Biophysics Reports 14 (2018) 58–63

Contents lists available at ScienceDirect

Biochemistry and Biophysics Reports

journal homepage: www.elsevier.com/locate/bbrep

# Analysis of the substrate recognition state of TDP-43 to single-stranded DNA using fluorescence correlation spectroscopy

Akira Kitamura[a], Ai Shibasaki[a], Kayo Takeda[a], Ryoji Suno[b], Masataka Kinjo[a,*]

[a] Laboratory of Molecular Cell Dynamics, Faculty of Advanced Life Science, Hokkaido University, Sapporo 001-0021, Japan
[b] Department of Cell Biology, Graduate School of Medicine, Kyoto University, Kyoto 605-8501, Japan

ARTICLE INFO

*Keywords:*
Transactivation response DNA/RNA-binding protein 43 kDa
Dissociation constant
Binding stoichiometry
Fluorescence correlation spectroscopy
Electrophoretic mobility shift assay

ABSTRACT

Normal function and abnormal aggregation of transactivation response (TAR) DNA/RNA-binding protein 43 kDa (TDP-43) are directly associated with the lethal genetic diseases: cystic fibrosis, amyotrophic lateral sclerosis (ALS), and frontotemporal lobar degeneration (FTLD). The binding of TDP-43 to single-stranded DNA (ssDNA) or RNA is involved in transcriptional repression, regulation of RNA splicing, and RNA stabilization. Equilibrium dissociation constants ($K_d$) of TDP-43 and ssDNA or RNA have been determined using various methods; however, methods that can measure $K_d$ with high sensitivity in a short time using a small amount of TDP-43 in solution would be advantageous. Here, in order to determine the $K_d$ of TDP-43 and fluorescence-labeled ssDNA as well as the binding stoichiometry, we use fluorescence correlation spectroscopy (FCS), which detects the slowed diffusion of molecular interactions in solution with single-molecule sensitivity, in addition to electrophoretic mobility shift assay (EMSA). Using tandem affinity chromatography of TDP-43 dually tagged with glutathione-S-transferase and poly-histidine tags, highly purified protein was obtained. FCS successfully detected specific interaction between purified TDP-43 and TG ssDNA repeats, with a $K_d$ in the nanomolar range. The $K_d$ of the TDP-43 mutant was not different from the wild type, although mutant oligomers, which did not bind ssDNA, were observed. Analysis of the fluorescence brightness per dimerized TDP-43/ssDNA complex was used to evaluate their binding stoichiometry. The results suggest that an assay combining FCS and EMSA can precisely analyze ssDNA recognition mechanisms, and that FCS may be applied for the rapid and quantitative determination of the interaction strength between TDP-43 and ssDNA or RNA. These methods will aid in the elucidation of the substrate recognition mechanism of ALS- and FTLD-associated variants of TDP-43.

## 1. Introduction

Transactivation response (TAR) DNA/RNA-binding protein 43 kDa (TDP-43, encoded by *TARDBP*) is a ubiquitously expressed protein, and its normal function and abnormal aggregation are directly associated with the lethal genetic disease cystic fibrosis, as well as two devastating neurodegenerative disorders: amyotrophic lateral sclerosis (ALS) and Tau-negative and TDP-43-positive frontotemporal lobar degeneration (FTLD-TDP) [1–3]. TDP-43 was first characterized as a transcriptional repressor bound to the TAR DNA sequence of the gene of HIV-1 [4]. TDP-43 also acts as a splicing factor, binding to the intron 8/exon 9 junction of the cystic fibrosis transmembrane conductance regulator (CFTR) gene [5]. TDP-43 prefers to bind TG-rich single-stranded DNA (ssDNA) or UG-rich RNA [6–8]. The sequence preference of TDP-43 for UG repeats in the splice sites of various pre-mRNA transcripts, such as POLDIP3/SKAR, sortilin 1, and DNAJC5, regulates exon exclusion and inclusion [6,7,9]. Interactions between TDP-43 and microRNAs/small RNAs maintain their stability and processing [10,11].

The cytoplasmic accumulation of TDP-43 aggregates in inclusion bodies (IBs) has been observed in motor neurons from patients with ALS and FTLD [12]. Many ALS- and FTLD-associated missense mutations, which cause amino acid substitutions, have been identified in the *TARDBP* gene [3]. These TDP-43 mutants are intimately involved in the onset and severity of ALS and FTLD. The ALS-associated mutation (A315T) promotes the formation of aggregates, leading to motor neuron loss [13]. In addition, TDP-43 knockdown increases the proportion of neuronal cell death [11]. Therefore, two hypotheses for motor neuron cell death, due to TDP-43 aggregates harboring cytotoxicity or loss of TDP-43 function, have been proposed [6,14].

TDP-43 carries 2 RNA/DNA-recognition motifs (RRM1 and RRM2) and a C-terminal glycine-rich region (GRR) including the prion-like intrinsically disordered region (IDR; also called the low complexity sequence domain), which regulates interactions with proteins (e.g., heterogeneous nuclear ribonucleoprotein A1/A2 and FUS RNA binding

* Corresponding author.
*E-mail address:* kinjo@sci.hokudai.ac.jp (M. Kinjo).

https://doi.org/10.1016/j.bbrep.2018.03.009
Received 8 March 2018; Received in revised form 28 March 2018; Accepted 30 March 2018
2405-5808/ © 2018 The Authors. Published by Elsevier B.V. This is an open access article under the CC BY-NC-ND license (http://creativecommons.org/licenses/BY-NC-ND/4.0/).

protein). TDP-43 dimerization via the N-terminal ubiquitin-like domain (NTD) has been reported [15].

The equilibrium dissociation constants ($K_d$) between TDP-43 and various ssDNA and RNA have been determined using cross-linking and immunoprecipitation followed by electrophoretic mobility shift assay (EMSA) [16], nitrocellulose filter binding assay [17], fluorescence quenching [18], surface plasmon resonance [19], and isothermal titration calorimetry [20]. The $K_d$ value of full-length TDP-43 or its RRMs with RNA containing 6 UG repeats is several nM, and decreases as the chain length increases [17,18]. However, the binding stoichiometry between TDP-43 and nucleic acids remains unclear. Moreover, establishment of a procedure that can rapidly measure $K_d$ in a solution even with a low yield protein such as TDP-43 is useful in the analysis of the binding state between TDP-43 and nucleic acids. Hence, we calculated the $K_d$ between TDP-43 and single-stranded 12 TG repeat ssDNA, and determined the binding stoichiometry using fluorescence correlation spectroscopy (FCS), which can determine $K_d$ and molecular brightness per single particle with single molecule sensitivity.

## 2. Materials & methods

### 2.1. Protein expression and purification

*Escherichia coli* BL21(DE3) cells carrying plasmids coding wild type (WT) or ALS-associated A315T mutant (AT) TDP-43 tagged with glutathione S-transferase (GST) at the N-terminus and poly-histidine (6× His) at the C-terminus (GST-TDP-43-His; Fig. 1A) were cultured in 2×YT medium containing 100 μg/mL ampicillin at 37 °C. When the optical density reached 0.45–0.5, the cells were cultured in medium containing 0.5 mM isopropyl β-D-1-thiogalactopyranoside (IPTG) for 2 h at 18 °C to induce protein expression. Harvested cells were lysed in buffer A (50 mM HEPES-KOH (pH 7.5), 150 mM NaCl, and 1 mM dithiothreitol (DTT)) containing 0.1% Triton-X 100 and protease inhibitor cocktail (TaKaRa, Shiga, Japan), and ultracentrifuged at 40,000 rpm for 1 h at 4 °C. The soluble fractions were recovered and transferred to glutathione sepharose columns (GSTrap HP; GE Healthcare, Chicago, IL, USA) in AKTA prime system (GE Healthcare). The columns were washed with buffer A and eluted in buffer A containing 10 mM reduced glutathione. The eluted solutions were transferred to nickel-nitrilotriacetic acid (Ni-NTA) columns (HisTrap HP; GE Healthcare) and washed in buffer A containing 20 mM imidazole; and then proteins were eluted in buffer A containing 500 mM imidazole. The buffer was replaced with 50 mM HEPES-KOH (pH 7.5) using a centrifugal dialysis filter (Amicon Ultra; Merck, Darmstadt, Germany), then 1% NP-40 was added if necessary.

### 2.2. FCS

FCS measurements were performed using a ConfoCor 2 system combined with an LSM 510 META confocal laser scanning microscope (Carl Zeiss, Jena, Germany) through a C-Apochromat 40×/1.2 NA Korr UV-VIS-IR water-immersion objective (Carl Zeiss). The confocal pinhole diameter was adjusted to 90 μm. Alexa Fluor 647 was excited at 633 nm and emission was detected using a 650-nm long-pass filter. Measurements were performed in a cover-glass chamber (#155411, Thermo Fisher Scientific, Waltham, MA) after mixing purified TDP-43 with 3.3 nM Alexa Fluor 647-labeled ssDNA carrying 12 TG repeats ($TG_{12}$) or 20 T repeats ($T_{20}$), synthesized by Thermo Fisher Scientific. The obtained fluorescence autocorrelation function (ACF), $G(\tau)$ (in which the lag time ($\tau$), was analyzed using a two-component diffusion model including the exponential relaxation state derived from dynamic fluorescence quenching, mainly accompanied with intersystem crossing between triplet and singlet state and photo-induced *cis-trans* isomerization of the Alexa Fluor 647 dye [21]) was given by Eq. (1):

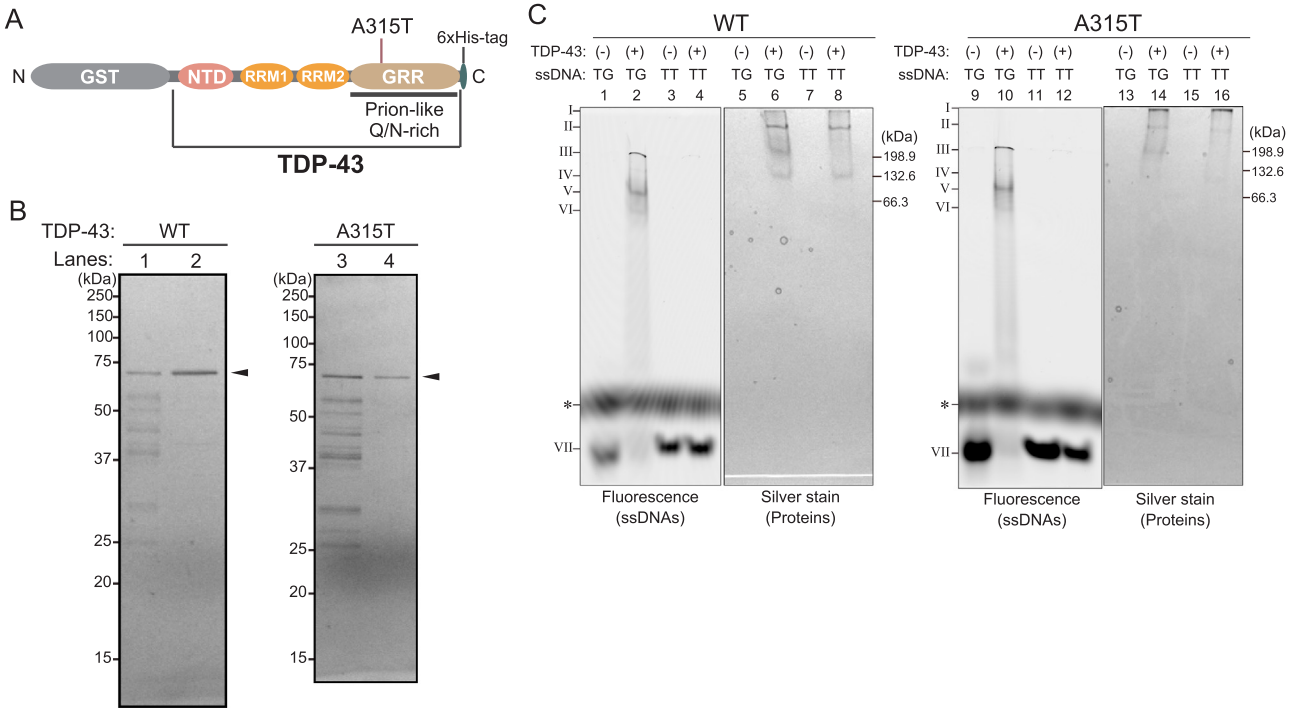


**Fig. 1. Single-strand DNA-binding activity of purified TDP-43.** (A) Primary structure of TDP-43 tagged with glutathione S-transferase (GST) and a 6× poly-histidine tag. NTD: N-terminal domain, RRM1/2: RNA/DNA-recognition motif 1/2, GRR: glycine-rich region (including the Q/N-rich and prion-like region). (B) Purification of wild type (WT) and ALS-associated A315T (AT) mutant GST-TDP-43-His using SDS-PAGE and silver staining. GST column elutes (lanes 1 & 3) and subsequent Ni-NTA column elutes (lanes 2 & 4) are shown. Arrowheads indicate GST-TDP-43-His. (C) Fluorescent and silver stained gel images. GST-TDP-43-His migration in the presence of $TG_{12}$ (TG) or $T_{20}$ (TT), and ssDNAs are shown. Molecular weights were determined from the migration of bovine serum albumin monomers, dimers, and trimers, as indicated on the right. The migrated positions of ssDNA and TDP-43 are indicated by bands I–VII. *, auto-fluorescence of bromophenol blue.

$$G(\tau) = 1+\frac{1}{N}\left[\frac{T}{1-T}\exp\left(-\frac{\tau}{\tau_{\mathrm{Relax}}}\right)\right]\left[\frac{1-F_{\mathrm{bound}}}{\left(1+\frac{\tau}{\tau_{\mathrm{free}}}\right)^{-1}\left(1+\frac{\tau}{s^2\tau_{\mathrm{free}}}\right)^{-\frac{1}{2}}} + \frac{F_{\mathrm{bound}}}{\left(1+\frac{\tau}{\tau_{\mathrm{bound}}}\right)^{-1}\left(1+\frac{\tau}{s^2\tau_{\mathrm{bound}}}\right)^{-\frac{1}{2}}}\right] \quad (1)$$

where $\tau_{\mathrm{free}}$ and $\tau_{\mathrm{bound}}$ are the diffusion times of free and bound molecules, respectively; $F_{\mathrm{bound}}$ denotes the binding fraction of Alexa Fluor 647-labeled ssDNAs; $N$ is the average number of fluorescent ssDNAs in the confocal detection volume, defined by the beam waist $w_0$ and the axial radius $z_0$; $s$ is a structure parameter representing the ratio of $w_0$ and $z_0$; $T$ is the exponential relaxation fraction; and $\tau_{\mathrm{Relax}}$ is the relaxation time of the state. $G(\tau)$ values were measured for 70 s. Following pinhole adjustment, the diffusion time ($\tau_{\mathrm{Rh6G}}$) and structure parameter ($s$) were determined using 0.1 μM Rhodamine 6 G (Rh6G) as a standard prior to measurements. The $w_0$ was determined using Eq. (2).

$$w_0 = \sqrt{4D_{\mathrm{Rh6G}}\cdot\tau_{\mathrm{Rh6G}}} \quad (2)$$

where $\tau_{\mathrm{Rh6G}}$ is the measured diffusion time of Rh6G, and $D_{\mathrm{Rh6G}}$ is the diffusion coefficient of Rh6G (414 $\mu m^2/s$). The volume element $V_{\mathrm{eff}}$ was calculated using Eq. (3).

$$V_{\mathrm{eff}} = \pi^{2/3} w_0^2 z_0 \quad (3)$$

Counts per particle (CPP) values, each indicating the fluorescence intensity of a single particle, were derived from Eq. (4).

$$\mathrm{CPP} = \frac{\langle I\rangle}{N} \quad (4)$$

where $< I >$ indicates the mean count rate.

### 2.3. Calculation of the apparent dissociation constant

The dissociation constant ($K_{\mathrm{d}}$) was calculated using Eq. (5).

$$K_{\mathrm{d}} = \frac{[Protein_{\mathrm{free}}][ssDNA_{\mathrm{free}}]}{[Complex]} \quad (5)$$

where, [$Protein_{\mathrm{free}}$] is the concentration of unbound protein, [$ssDNA_{\mathrm{free}}$] is the concentration of unbound ssDNA, and [$Complex$] is the concentration of the complex, as per Eqs. 6, 7, and 8.

$$[Complex] = F_{bound}\cdot N\cdot N_A^{-1}\cdot V_{eff}^{-1} \quad (6)$$

$$[ssDNA_{\mathrm{free}}] = [ssDNA_{\mathrm{total}}] - [Complex] \quad (7)$$

$$[Protein_{\mathrm{free}}] = [Protein_{\mathrm{total}}] - [Complex] \quad (8)$$

where $N_{\mathrm{A}}$ is Avogadro constant, [$ssDNA_{\mathrm{total}}$] was obtained from FCS, and [$Protein_{\mathrm{total}}$] was obtained from the bovine serum albumin (BSA) calibration curve using silver staining.

### 2.4. EMSA

Alexa Fluor 647-labeled ssDNA ($TG_{12}$ or $T_{20}$) was combined with either purified TDP-43 in a sample buffer containing 50 mM HEPES-KOH (pH 7.5) and 10% glycerol or with buffer alone, and resolved on 7.5% polyacrylamide gels including 375 mM HEPES-KOH (pH 7.5). Electrophoresis was performed in a running buffer including 35 mM HEPES and 43 mM imidazole at 120 V and 4 °C. After the infrared fluorescence of the ssDNAs in the gels was captured using a Typhoon fluorescence image scanner (Thermo Fisher Scientific), TDP-43 in the gel was visualized using silver staining (Cosmo Bio Co. Ltd., Tokyo, Japan).

## 3. Results

### 3.1. Purification of recombinant TDP-43 possessing single-strand DNA (ssDNA)-binding ability

We initially attempted to purify GST-TDP43WT-His (TDP-43WT) using the GST tag; however, the sample eluted from the glutathione sepharose column included many fragments of TDP-43WT in addition to the full-length protein (Fig. 1B, lane 1). We therefore further purified the protein by Ni-NTA sepharose affinity chromatography. Tandem affinity chromatography successfully produced highly purified TDP-43WT (Fig. 1B, lane 2) as well as GST-TDP43-A315T-His (TDP-43AT) (Fig. 1B, lanes 3 & 4). These results indicated that the fragments of TDP-43 truncated at the C-terminus. Truncation patterns between the WT and AT mutant proteins were not changed.

To confirm whether the purified TDP-43 proteins were correctly folded, their specific ssDNA (TG repeat)-binding ability was examined using EMSA. $TG_{12}$ migrated more slowly in the presence of WT or AT mutant TDP-43 than in their absence (bands III, V, and VI; Fig. 1C, lanes 1, 2, 9, and 10), whereas $T_{20}$ migration was not slowed in the presence of TDP-43 (band VII; Fig. 1C, lanes 3, 4, 11, and 12). Band III was observed in the silver stained gel, whereas bands V and VI were not (Fig. 1C, lanes 6 and 14), indicating that band III is the TDP-43/$TG_{12}$ complex, and that a portion of $TG_{12}$ may have dissociated during electrophoresis. These results confirmed that both WT and AT mutant TDP-43 maintained specific ssDNA-binding ability.

### 3.2. Determination of the $K_d$ between TDP-43 and ssDNA

To observe interactions between TDP-43 and fluorescence-labeled ssDNA in solution, we employed FCS, which can detect molecular interactions by measuring the apparent increased molecular weight of low molecular weight fluorescent molecules though their decreased diffusion speed when bound to high molecular weight species in solution with single molecule sensitivity [22,23]. The autocorrelation functions (ACFs) of $TG_{12}$ were shifted to the right in the presence of purified WT and AT mutant TDP-43, whereas those of $T_{20}$ were not (Fig. 2), indicating specific interactions between purified TDP-43 and $TG_{12}$.

Next, to quantify the interaction strength between TDP-43 and $TG_{12}$, we calculated $K_{\mathrm{d}}$ values using FCS. Complex and unbound molecule concentrations were obtained through FCS measurement of each sample and calculated using Eqs. 6, 7, and 8, and linear regression calculations were performed to determine the fitting line through each scatter plot. $K_{\mathrm{d}}$ values were calculated from the slope of the regression line. The $K_{\mathrm{d}}$ value between TDP-43WT and $TG_{12}$ in the absence of NP-40, a detergent, did not differ from that of the AT mutant 237 ± 39.4 and 289 ± 21.4 nM, respectively; slope value ± standard error of the mean (SEM; Fig. 3A). Although the $K_{\mathrm{d}}$ values of WT and AT TDP-43 with $TG_{12}$ were decreased in the presence of NP-40 (90.0 ± 5.3 and 89.2 ± 6.0 nM, respectively), differences between the WT and AT mutant proteins were not observed (Fig. 3B). Moreover, the $K_{\mathrm{d}}$ value between TDP-43 wt and $TG_{12}$ in the absence of NP-40 was dramatically increased after storage at 4 °C for 1 day after the purification; however, in presence of NP-40, the $K_{\mathrm{d}}$ value was not changed in the same storage conditions (Supplemental Figure), suggesting that NP-40 stabilized TDP-43. These results suggest that the ssDNA-binding ability of wild type TDP-43 may not differ from that of the ALS-associated A315T mutant of TDP-43, and that this ability may be involved in the active structure of TDP-43.

### 3.3. Stoichiometry of TDP-43/ssDNA binding

Three migration patterns for purified TDP-43 were observed when not bound to ssDNA (bands I, II, and IV, Fig. 1C, lanes 8 and 16). The migration of band IV corresponded to that of BSA dimers (132.6 kDa;

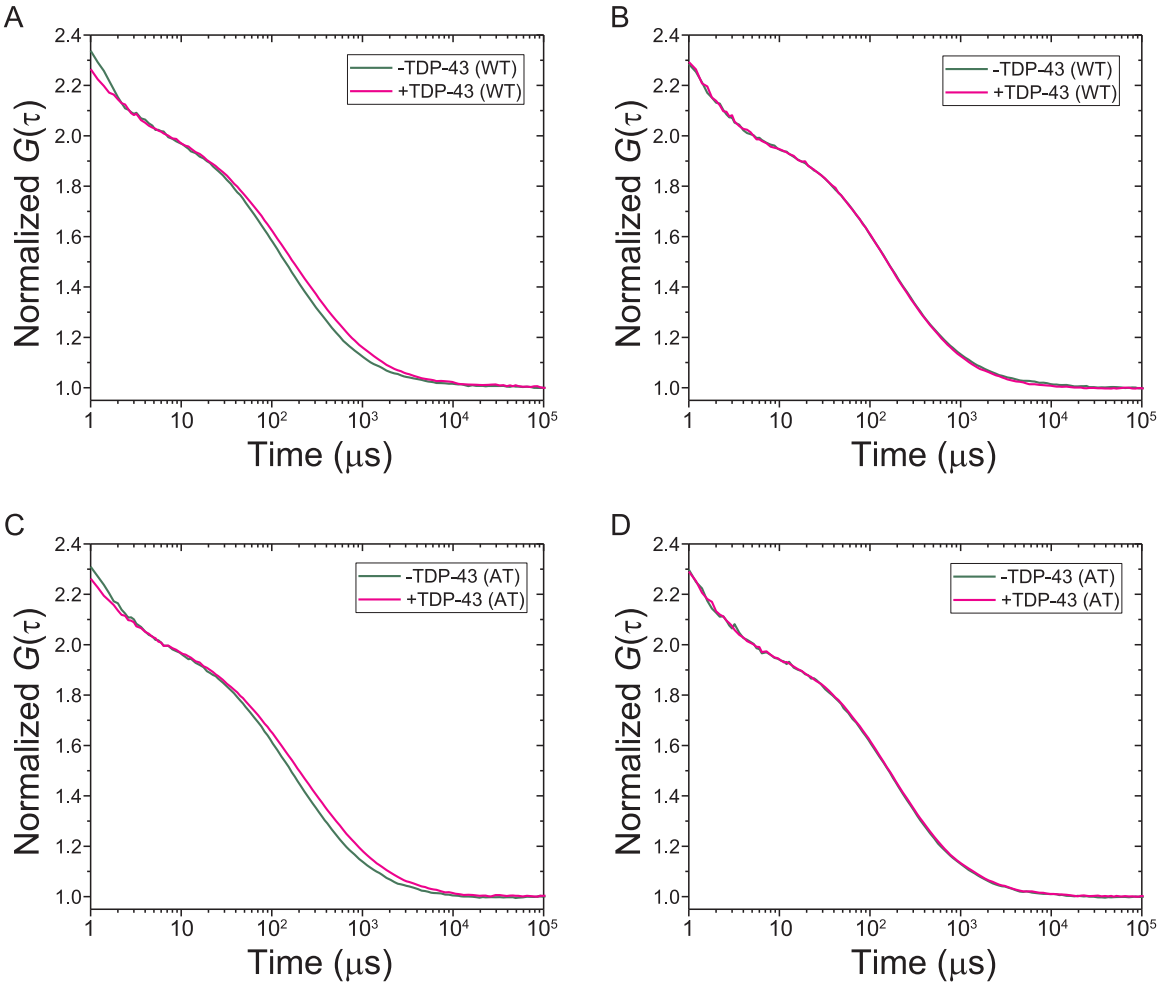


**Fig. 2. Autocorrelation functions (ACFs) of fluorescently labeled ssDNA in the presence and absence of purified TDP-43.** Normalized ACFs of Alexa Fluor 647-labeled $TG_{12}$ (TG; A & C) or $T_{20}$ (TT; B & D) in 50 mM HEPES-KOH buffer without NP-40 are shown in the presence and absence of wild type TDP-43 (WT; 42.1 ng) or the A315T mutant (AT; 67.5 ng; magenta and green, respectively).

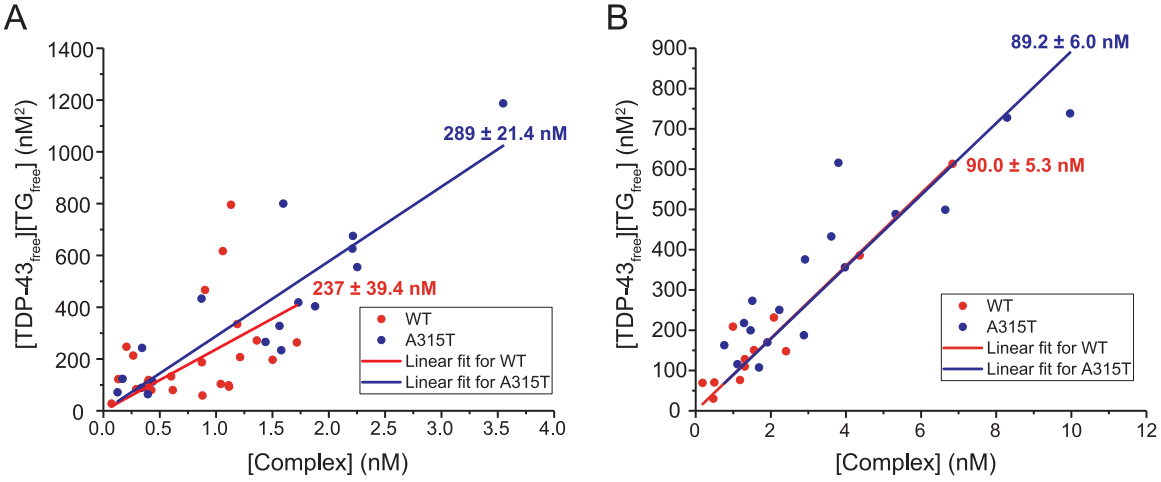


**Fig. 3. Determination of the $TG_{12}$/TDP-43 dissociation constant using FCS.** (A and B) $K_d$ determinations using scatter plots and linear regression in the absence (A) or presence (B) of NP-40. The plot represents the concentration of free $TG_{12}$ and TDP-43 versus the concentration of the TDP-43/$TG_{12}$ complex. The red and blue solid dots show each measurement result for wild type and A315T mutant, respectively. The sample size: (A) wild type (n = 24) and A315T (n = 18), (B) wild type (n = 12) and A315T (n = 17). The red and blue solid lines show the linear fit for wild type and A315T mutant TDP-43, respectively. The slope represents the $K_d$, and inset values represent the slope ± SEM. (For interpretation of the references to color in this figure legend, the reader is referred to the web version of this article)

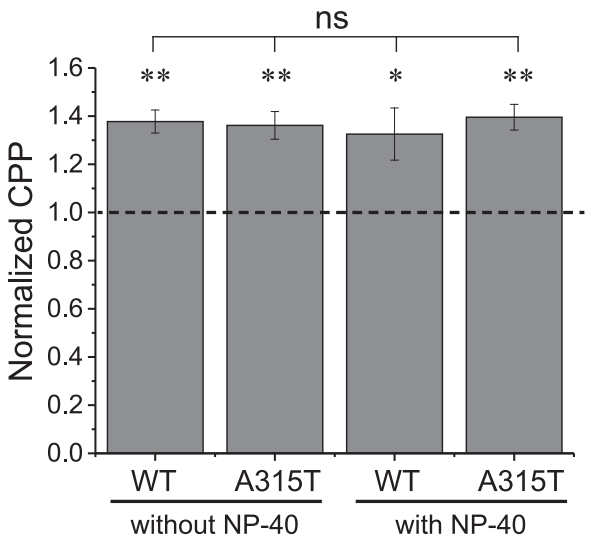


**Fig. 4. Binding stoichiometry of TDP-43 and ssDNA.** Normalized counts per particle (CPP) values of Alexa Fluor 647-labeled $TG_{12}$ in the presence of TDP-43 (mean ± SEM; n = 3). The dotted line indicates the CPP value in the absence of TDP-43. Student's *t*-test was used to compare values in the presence and absence of TDP-43; $*p < 0.05$ and $**p < 0.01$. No significant difference: ns.

Fig. 1C, lanes 8 and 16), and the theoretical monomeric molecular weight of GST-tagged TDP-43 was 73.5 kDa; thus, TDP-43 migrated as a dimer. TDP-43 migrated more slowly than BSA trimers (band II; Fig. 1C, lanes 8 and 16), suggesting that a portion of TDP-43 may form tetramers or higher order multimers. Moreover, the intensity of the band of TDP-43AT at the initial sample loading point (band I) was increased comparing to that of wild type, suggesting that TDP-43AT has a greater tendency to oligomerize compared to the WT protein. Since $TG_{12}$ was not found in the electrophoresis position of these TDP-43 oligomers (bands I and II), they may be aggregated. The estimated molecular weight of the TDP-43-$TG_{12}$ complex (band III) corresponded to that of BSA trimers (198.9 kDa). Therefore, the TDP-43-$TG_{12}$ complex included TDP-43 dimers.

FCS analysis can determine the mean fluorescence brightness per particle (CPP); thus, it is possible to investigate the number of ssDNAs contained in the TDP-43-$TG_{12}$ complex. The CPP values of $TG_{12}$ in the presence of WT or AT mutant TDP-43 were significantly higher than those in absence of TDP-43 (Fig. 4). FCS analysis using a two-component diffusion model indicated that the proportion of the TDP-43-$TG_{12}$ complex was approximately 40%, which corresponds to that calculated from the increase CPP ratio, assuming that the TDP-43 dimers include two molecules of $TG_{12}$. Therefore, the TDP-43-TG12 complex including TDP-43 dimers may exist predominantly in a 1:1 ratio.

## 4. Discussion

We have successfully determined the apparent $K_d$ between recombinant full-length TDP-43 and TG ssDNA repeat using FCS in solution and EMSA, providing a high accuracy molecular weight separation method. Although various determinations of the $K_d$ between TDP-43 and RNA/DNA using biochemical or fluorescence-based methods have been reported, using FCS allows the $K_d$ to be rapidly measured in a native solution state. The $K_d$ between recombinant full-length TDP-43 and 6 UG repeat RNA, calculated using the fluorescence quenching of TDP-43 as a titration of the RNA, was reported to be several nM [18,24], lower than our result in spite of the use of a longer twelve TG repeat DNA (~90 nM in the presence of NP-40; Fig. 3B). This may be because only a portion of TDP-43 is bound to $TG_{12}$. In fact, taking into account that approximately 50% of the TDP-43 bound to ssDNA according to EMSA, and the ~8-fold higher $K_d$ of the TDP-43 RRM with DNA compared with RNA [17], the corrected $K_d$ corresponds to ~5.6 nM. Therefore, the $K_d$ value was not inferior to the obtained value using FCS. Otherwise, in the previous work, TDP-43 oligomers might bind with $TG_{12}$ more stable than dimers depending on different expression and purification condition, causing the much lower $K_d$.

We found that NP-40 stabilized the purified TDP-43. The binding activity of TDP-43 was decreased in the absence of NP-40 with unchanged concentration 1 d after the purification (Supplemental Figure), suggesting that the deactivation of ssDNA binding ability is not due to fragmentation and degradation of the protein. The stabilization of TDP-43 through inter-domain interactions and the adoption of a closed conformation, as well as self-assembly of the C-terminal IDR at neutral pH, have been reported [25,26]. NP-40 may stabilize the TDP-43 structure by preventing C-terminal IDR self-assembly even at neutral pH.

The $K_d$ value of the ALS-associated A315T mutant of TDP-43 was not different from that of the WT (Fig. 3, A and B). Although the binding affinity of TDP-43 to UG/TG-rich RNA/DNA is mainly mediated through the RRM [8,16,17], NMR analysis shows that the C-terminal IDR and NTD of TDP-43 can bind to TG repeat ssDNA. Thus, the C-terminal IDR and NTD of TDP-43 may be secondarily involved in binding RNA/DNA, possibly by capturing long nucleic acid strands bound to the RRM. In fact, TDP-43 carrying the M337V mutation binds weakly to PSD-95 and CaMKIIa mRNA [19]. Therefore, the ALS-associated mutations in the C-terminal IDR may not dramatically affect binding affinity to short nucleic acid strands; however, they would affect binding to long nucleic acid strands such as mRNAs or long non-coding RNAs.

The multimerization of TDP-43 in mammalian cells as well as in solution has been reported [27–29]. Dimerization occurs though homodimerization of the TDP-43 NTD [30]. However, it is difficult to distinguish dimers, trimers, and higher multimers in sample due to the propensity of TDP-43 to aggregate. Our established purification system provides recombinant TDP-43 with good solubility and ssDNA-binding ability, and demonstrates that a portion of TDP-43 forms dimers, and that two ssDNAs bind to each dimer. Thus, the interaction stoichiometry between TDP-43 dimers and ssDNA appears to be 1:1.

Finally, we established a rapid measurement system at the uL scale using nM levels of purified TDP-43 and fluorescently labeled nucleic acids by FCS. This system can be applied to high throughput and quantitative determinations of interactions between TDP-43 and ssDNA or RNA to elucidate the substrate recognition mechanism of ALS-associated TDP-43.

## Acknowledgements

A.K. was supported by a Japan Society for Promotion of Science (JSPS) Grant-in-Aid for the Promotion of Joint International Research (Fostering Joint International Research) (16KK0156); a JSPS Grant-in-Aid for Scientific Research (C) (#26440090); by a grant-in-aid from The Nakabayashi Trust for ALS research (Tokyo, Japan); by a grant-in-aid from the Japan Amyotrophic Lateral Sclerosis Association (JALSA, Tokyo, Japan) for ALS research, and by a grant from the Akiyama Life Science Foundation (Sapporo, Japan).

## Author contributions

Conceived and designed the experiments: AK. Developed the protein purification: AK, AS, and RS. Developed measurement conditions to detect protein-DNA interactions: AK and AS. Performed the fluorescence correlation spectroscopy: AK, AS, and KT. Analyzed the data: AK, AS, KT, and MK. Wrote the paper: AK and MK.

## Appendix A. Transparency document

Supplementary data associated with this article can be found in the

online version at http://dx.doi.org/10.1016/j.bbrep.2018.03.009.

## References


[1] E. Buratti, F.E. Baralle, The multiple roles of TDP-43 in pre-mRNA processing and gene expression regulation, RNA Biol. 7 (2010) 420–429.

[2] A. Ratti, E. Buratti, Physiological functions and pathobiology of TDP-43 and FUS/TLS proteins, J. Neurochem. 138 (Suppl 1) (2016) 95–111.

[3] C. Lagier-Tourenne, M. Polymenidou, D.W. Cleveland, TDP-43 and FUS/TLS: emerging roles in RNA processing and neurodegeneration, Hum. Mol. Gen. 19 (2010) R46–R64.

[4] S.H. Ou, F. Wu, D. Harrich, L.F. Garcia-Martinez, R.B. Gaynor, Cloning and characterization of a novel cellular protein, TDP-43, that binds to human immunodeficiency virus type 1 TAR DNA sequence motifs, J. Virol. 69 (1995) 3584–3596.

[5] E. Buratti, T. Dork, E. Zuccato, F. Pagani, M. Romano, F.E. Baralle, Nuclear factor TDP-43 and SR proteins promote in vitro and in vivo CFTR exon 9 skipping, EMBO J. 20 (2001) 1774–1784.

[6] M. Polymenidou, C. Lagier-Tourenne, K.R. Hutt, S.C. Huelga, J. Moran, T.Y. Liang, S.C. Ling, E. Sun, E. Wancewicz, C. Mazur, H. Kordasiewicz, Y. Sedaghat, J.P. Donohue, L. Shiue, C.F. Bennett, G.W. Yeo, D.W. Cleveland, Long pre-mRNA depletion and RNA missplicing contribute to neuronal vulnerability from loss of TDP-43, Nat. Neurosci. 14 (2011) 459–468.

[7] J.R. Tollervey, T. Curk, B. Rogelj, M. Briese, M. Cereda, M. Kayikci, J. Konig, T. Hortobagyi, A.L. Nishimura, V. Zupunski, R. Patani, S. Chandran, G. Rot, B. Zupan, C.E. Shaw, J. Ule, Characterizing the RNA targets and position-dependent splicing regulation by TDP-43, Nat. Neurosci. 14 (2011) 452–458.

[8] P.H. Kuo, C.H. Chiang, Y.T. Wang, L.G. Doudeva, H.S. Yuan, The crystal structure of TDP-43 RRM1-DNA complex reveals the specific recognition for UG- and TG-rich nucleic acids, Nucleic Acids Res. 42 (2014) 4712–4722.

[9] A. Shiga, T. Ishihara, A. Miyashita, M. Kuwabara, T. Kato, N. Watanabe, A. Yamahira, C. Kondo, A. Yokoseki, M. Takahashi, R. Kuwano, A. Kakita, M. Nishizawa, H. Takahashi, O. Onodera, Alteration of POLDIP3 splicing associated with loss of function of TDP-43 in tissues affected with ALS, PLOS One 7 (2012) e43120.

[10] Y. Kawahara, A. Mieda-Sato, TDP-43 promotes microRNA biogenesis as a component of the Drosha and Dicer complexes, Proc. Natl. Acad. Sci. USA 109 (2012) 3347–3352.

[11] M. Yahara, A. Kitamura, M. Kinjo, U6 snRNA expression prevents toxicity in TDP-43-knockdown cells, PLOS One 12 (2017) e0187813.

[12] M. Neumann, D.M. Sampathu, L.K. Kwong, A.C. Truax, M.C. Micsenyi, T.T. Chou, J. Bruce, T. Schuck, M. Grossman, C.M. Clark, L.F. McCluskey, B.L. Miller, E. Masliah, I.R. Mackenzie, H. Feldman, W. Feiden, H.A. Kretzschmar, J.Q. Trojanowski, V.M. Lee, Ubiquitinated TDP-43 in frontotemporal lobar degeneration and amyotrophic lateral sclerosis, Science 314 (2006) 130–133.

[13] L. Bargsted, D.B. Medinas, F. Martinez Traub, P. Rozas, N. Munoz, M. Nassif, C. Jerez, A. Catenaccio, F.A. Court, C. Hetz, S. Matus, Disulfide cross-linked multimers of TDP-43 and spinal motoneuron loss in a TDP-43(A315T) ALS/FTD mouse model, Sci. Rep. 7 (2017) 14266.

[14] Y.S. Fang, K.J. Tsai, Y.J. Chang, P. Kao, R. Woods, P.H. Kuo, C.C. Wu, J.Y. Liao, S.C. Chou, V. Lin, L.W. Jin, H.S. Yuan, I.H. Cheng, P.H. Tu, Y.R. Chen, Full-length TDP-43 forms toxic amyloid oligomers that are present in frontotemporal lobar dementia-TDP patients, Nat. Commun. 5 (2014) 4824.

[15] H. Qin, L.Z. Lim, Y. Wei, J. Song, TDP-43 N terminus encodes a novel ubiquitin-like fold and its unfolded form in equilibrium that can be shifted by binding to ssDNA, Proc. Natl. Acad. Sci. USA 111 (2014) 18619–18624.

[16] A. Bhardwaj, M.P. Myers, E. Buratti, F.E. Baralle, Characterizing TDP-43 interaction with its RNA targets, Nucleic Acids Res. 41 (2013) 5062–5074.

[17] P.H. Kuo, L.G. Doudeva, Y.T. Wang, C.K. Shen, H.S. Yuan, Structural insights into TDP-43 in nucleic-acid binding and domain interactions, Nucleic Acids Res. 37 (2009) 1799–1808.

[18] W. Li, A.N. Reeb, B. Lin, P. Subramanian, E.E. Fey, C.R. Knoverek, R.L. French, E.H. Bigio, Y.M. Ayala, Heat shock-induced phosphorylation of TAR DNA-binding protein 43 (TDP-43) by MAPK/ERK kinase regulates TDP-43 function, J. Biol. Chem. 292 (2017) 5089–5100.

[19] A. Ishiguro, N. Kimura, Y. Watanabe, S. Watanabe, A. Ishihama, TDP-43 binds and transports G-quadruplex-containing mRNAs into neurites for local translation, Genes Cells 21 (2016) 466–481.

[20] P.J. Lukavsky, D. Daujotyte, J.R. Tollervey, J. Ule, C. Stuani, E. Buratti, F.E. Baralle, F.F. Damberger, F.H. Allain, Molecular basis of UG-rich RNA recognition by the human splicing factor TDP-43, Nature Struct. Mol. Biol. 20 (2013) 1443–1449.

[21] J. Widengren, P. Schwille, Characterization of photoinduced isomerization and back-isomerization of the cyanine dye Cy5 by fluorescence correlation spectroscopy, J. Phys. Chem. A 104 (2000) 6416–6428.

[22] A. Kitamura, Y. Ishida, H. Kubota, C.G. Pack, T. Homma, S. Ito, K. Araki, M. Kinjo, K. Nagata, Detection of substrate binding of a collagen-specific molecular chaperone HSP47 in solution using fluorescence correlation spectroscopy, Biochemi. Biophys. Res. Commun. 497 (2018) 279–284.

[23] R. Rigler, U. Mets, J. Widengren, P. Kask, Fluorescence correlation spectroscopy with high count rate and low-background - analysis of translational diffusion, Eur. Biophys. J. 22 (1993) 169–175.

[24] Y.M. Ayala, S. Pantano, A. D'Ambrogio, E. Buratti, A. Brindisi, C. Marchetti, M. Romano, F.E. Baralle, Human, Drosophila, and C.elegans TDP43: nucleic acid binding properties and splicing regulatory function, J. Mol. Biol. 348 (2005) 575–588.

[25] Y. Wei, L. Lim, L. Wang, J. Song, Inter-domain interactions of TDP-43 as decoded by NMR, Biochem. Biophys. Res. Commun. 473 (2016) 614–619.

[26] L. Lim, Y. Wei, Y. Lu, J. Song, ALS-causing mutations significantly perturb the self-assembly and interaction with nucleic acid of the intrinsically disordered prion-like domain of TDP-43, PLOS Biol. 14 (2016) e1002338.

[27] Y. Shiina, K. Arima, H. Tabunoki, J. Satoh, TDP-43 dimerizes in human cells in culture, Cell. Mol. Neurobiol. 30 (2010) 641–652.

[28] C. Foglieni, S. Papin, A. Salvade, T. Afroz, S. Pinton, G. Pedrioli, G. Ulrich, M. Polymenidou, P. Paganetti, Split GFP technologies to structurally characterize and quantify functional biomolecular interactions of FTD-related proteins, Sci. Rep. 7 (2017) 14013.

[29] T. Afroz, E.M. Hock, P. Ernst, C. Foglieni, M. Jambeau, L.A.B. Gilhespy, F. Laferriere, Z. Maniecka, A. Pluckthun, P. Mittl, P. Paganetti, F.H.T. Allain, M. Polymenidou, Functional and dynamic polymerization of the ALS-linked protein TDP-43 antagonizes its pathologic aggregation, Nat. Commun. 8 (2017) 45.

[30] L.L. Jiang, W. Xue, J.Y. Hong, J.T. Zhang, M.J. Li, S.N. Yu, J.H. He, H.Y. Hu, The N-terminal dimerization is required for TDP-43 splicing activity, Sci. Rep. 7 (2017) 6196.